Coarsening and accelerated equilibration in mass-conserving heterogeneous nucleation

Tom Chou[1] and Maria R. D'Orsogna[2]

[1]*Deptartments of Biomathematics and Mathematics, UCLA, Los Angeles, CA 90095-1766, USA*

[2]*Department of Mathematics, CSUN, Los Angeles, CA 91330-8313, USA*

We propose a model of mass-conserving heterogeneous nucleation to describe the dynamics of ligand-receptor binding in closed cellular compartments. When the ligand dissociation rate is small, competition among receptors for free ligands gives rise to two very different long-time ligand-receptor cluster-size distributions. Cluster sizes first plateau to a long-lived, initial-condition-dependent, "metastable" distribution, and coarsen only much later to a qualitatively different equilibrium one. Surprisingly, we also find parameters for which a very special subset of clusters have equal metastable and equilibrium sizes, appearing to equilibrate much faster than the rest. Our results provide a quantitative framework for ligand-binding kinetics and suggest a mechanism by which different clusters can approach their equilibrium sizes in unexpected ways.

PACS number(s): 64.60.Q−, 02.30.Hq, 05.70.Ln, 82.60.Nh

I. INTRODUCTION

The binding of multiple particles to specific nucleation sites is a key process in many physical and chemical settings. The formation of droplets, condensates on aerosols [1,2], and crystals [3] is often triggered by the presence of impurities or boundaries, in a process known as heterogeneous nucleation [4,5]. Heterogeneous nucleation also occurs in cell biology during the assembly of sickle hemoglobin [6], β-amyloid fibers [7], Arp2/3 complex-mediated actin nucleation [8], and probably during clathrin-coat assembly [9]. Within biochemical applications, ligand-receptor binding can also be viewed as a particular paradigm of heterogeneous nucleation, where multiple ligands bind to a single receptor akin to an impurity seed in solid-state nucleation.

Viewed through this lens, nucleation is ubiquitous in cell biology. Indeed, receptor loading levels control a variety of biochemical reactions, from viral entry to cell signaling. The chemical stoichiometries involved in ligand-binding events however, may limit the maximum number of ligands a receptor can hold to about a dozen. For example, hemoglobin can bind at most four oxygen molecules [10], virus-cell fusion occurs after a small number of cell surface receptors bind to a viral protein [11], and cell signaling is initiated after a certain number of phosphates bind to specific enzymes [12]. This is in contrast to most physical and chemical systems, in which aggregation of an unlimited number of particles can lead to the emergence of macroscopic structures.

An even more critical feature of nucleation in cellular settings is the small system volumes involved and, as a consequence, the presence of a finite number of monomeric ligands driving the nucleation process. In the small volumes encountered in cells, ligand production and degradation are often slower processes than attachment and detachment to receptors, allowing certain ligands to be depleted [13]. Because there is no source to replenish the free ligand concentration, receptors in confined, isolated systems compete amongst themselves for the finite pool of free monomeric ligands, as depicted in Fig. 1. For simplicity, throughout the remainder of this paper, the terms "monomers" and "ligands" will be used interchangeably, as will "seeds" and "receptors."

The dynamics of mass-conserving *homogeneous* nucleation has been well-studied in the context of Becker-Döring equations [14–16]. In this work we study its *heterogeneous* counterpart, relevant for ligand-receptor kinetics in biology. So far, most theoretical treatments for heterogeneous nucleation have considered equilibrium partition functions for nucleation with specific forms for the free energy of monomer association [17–19]. Many other approaches focus on either the molecular details and geometry of an individual cluster particle [20], or on the asymptotic dynamics of even more coarse-grained continuum size distributions [21]. In many applications, a constant source of monomers is also imposed [22]. Here, we will instead consider the dynamics of a system with a total fixed number M of monomeric ligands (bound and unbound) and a fixed number N_s of receptor seeds. Each receptor can bind at the most N monomeric ligands according to the spatially uniform mass-action equations we describe in the next section.

Two qualitatively different cases are analyzed. In Sec. III, we first consider irreversible binding, where the detachment rate is strictly zero so that once attached, monomers cannot detach from clusters. Irreversibility leads to a loss of ergodicity since only a fraction of the possible cluster configurations will be sampled during the dynamics, while many others will never be visited. As a result, the final "quenched" or "metastable" cluster-size distribution is not an equilibrium one and depends strongly on initial conditions. Ergodicity is restored in the case of a nonzero detachment rate, where all possible cluster configurations are eventually sampled and where the cluster sizes approach an equilibrium distribution, independent of the initial configuration. Reversible binding, in the limit of small unbinding rates, is in analyzed Sec. IV.

Several studies of homogeneous nucleation have shown the existence of long-lived metastable states followed by final equilibration, or "coarsening," to a very different cluster size distribution. These results were found for nucleating systems driven by an infinite supply of monomers and while allowing clusters to grow without bound [14,15,23]. Our results for mass-conserving heterogeneous nucleation show a similar coarsening behavior. The steady-state cluster distributions arising from the irreversible and reversible dynamics are very different from each other, especially in the limit of small
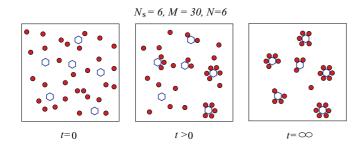
$N_s = 6, M = 30, N=6$

FIG. 1. (Color online) A heterogeneous nucleation process in which ligand monomers bind only to seeds. Here, $N_s = 6$ seeds (open hexagons) are available to bind $M = 30$ initial monomers (filled dots).

II. MASS-ACTION EQUATIONS

To begin our analysis, we consider a model of heterogeneous nucleation for M well-mixed monomeric ligands binding sequentially [24] to any of the N_s uniformly dispersed ligand seeds, neglecting fragmentation and aggregation that do not involve monomers, since they have been treated in other contexts [16,25]. We also assume that each seed can accommodate at most N monomers due to stoichiometry constraints, and consider the mean-field mass-action equations for the number of clusters $c_k(t)$ of size k, where $0 \leqslant k \leqslant N$. Here, $k = 0$ indicates "naked seeds," with no bound monomers, and $k = N$ saturated ones, where no further binding is possible. In general, monomer attachment and detachment rates from a cluster of size k can be explicitly k-dependent. Specific forms for p_k and q_k have been used to describe cooperativity and the nucleation of clusters of various shapes and in different dimensions. For instance, $p_k \sim k^{1/2}$ and constant q_k are typically used to model 2D nucleation of circular droplets when monomer binding is not diffusion-limited [26]. Here, we assume that while detachment is independent of the number of particles in the free monomer pool, the attachment process depends only

on how many monomers remain unbound. The Becker-Döring equations for $c_k(t)$ can thus be written as

$$\dot{c}_0 = -p_0 m(t) c_0 + q_1 c_1,$$
$$\dot{c}_k = -p_k m(t) c_k - q_k c_k + p_{k-1} m(t) c_{k-1} + q_{k+1} c_{k+1}, \quad (1)$$
$$\dot{c}_N = -q_N c_N + p_{N-1} m(t) c_{N-1}.$$

The rates $p_k m(t)$ and q_k represent monomer attachment and detachment rates, respectively. The effective attachment rate is proportional to $m(t)$, the number of free monomers available for binding:

$$m(t) \equiv M - \sum_{k=1}^{N} k c_k(t). \quad (2)$$

Note that although these equations are written assuming finite particle numbers, they can also describe concentrations, given a normalizing reference concentration. The quantities M, N, N_s, and $c_k(t)$ therefore need not be integers. We assume a typical initial condition where all the mass is in the form of monomers $m(t = 0) = M, c_0(t = 0) = N_s$, and $c_{k>0}(t = 0) = 0$. The other constraint particles must obey is that the total number of seeds must be N_s at all times, regardless of cluster population levels. We thus impose

$$N_s = \sum_{j=0}^{N} c_j(t), \quad (3)$$

which is satisfied by the system in Eq. (1), using the given initial conditions. For clarity, and because we will be referring to these equations often, we rewrite our mass-action equations for the simplified case of uniform attachment and detachment rates $p_k = p$ and $q_k = q$. This approximation might be most relevant for modeling nucleation and growth of linear filaments, where there are always only one or two ends that monomers can bind to or detach from. Rescaling time by the attachment rate p, we find

$$\dot{c}_0 = -m(t) c_0 + \varepsilon c_1,$$
$$\dot{c}_k = -m(t) c_k - \varepsilon c_k + m(t) c_{k-1} + \varepsilon c_{k+1}, \quad (4)$$
$$\dot{c}_N = -\varepsilon c_N + m(t) c_{N-1},$$

where $\varepsilon = q/p$. In the context of Eqs. (4), irreversible binding corresponds to $\varepsilon = 0$ and reversible binding to $\varepsilon > 0$. In the following, we shall be interested in the difference in behavior between $\varepsilon = 0$ and $\varepsilon \to 0^+$. As we shall see, the presence of a vanishingly small detachment rate $\varepsilon \to 0^+$ can lead to qualitatively different cluster-size distributions compared to those obtained in the purely irreversible case at $\varepsilon = 0$.

III. IRREVERSIBLE BINDING

We first consider the strictly irreversible binding limit in the general framework of Eqs. (1), where there is no detachment and $q_k = 0$. Two possibilities arise. For $M \geqslant N N_s$, there is an excess of available monomers. Given the irreversible nature of the dynamics, all N_s seeds will be fully occupied by N ligands, leaving $M - N N_s$ free ones. In this case, we expect steady-state solutions to yield $c_N(t \to \infty) = N_s$, $c_{k \neq N}(t \to \infty) = 0$, and $m(t \to \infty) = M - N N_s$. We shall call this the excess monomer limit. In the other case of $M < N N_s$ there are

particle numbers and even in the case of vanishingly small detachment rates. In the latter case, when unbinding is very slow compared to binding, relaxation to the true equilibrium cluster-size distribution occurs over the long time scales associated with unbinding. As a result, cluster concentrations reach long-lived metastable plateaus that depend on initial conditions and that can be closely approximated by results obtained from considering irreversible dynamics, as treated in Sec. III. Only at longer times, after monomers start unbinding in appreciable numbers, does this metastable size distribution "coarsen" and cross over to the true equilibrium one. While the metastable and equilibrium cluster distributions are generally very different, we find a surprising result: for certain sets of parameters, special cluster sizes have identical metastable and equilibrium concentrations. For these clusters, the equilibration process appears to be dramatically accelerated. In Sec. V we find the exact mathematical relationship leading to the apparent fast coarsening where certain clusters reach equilibrium concentrations well before the rest. Our results are a consequence of total mass conservation, and do not arise in the case of receptors binding an unlimited supply of free ligand monomers. Finally, in the Conclusions, we discuss implications and future extensions of our work.

not enough monomers to fill seeds to capacity, and a nontrivial steady state will arise. Here, we expect the existence of a finite time t_* at which the pool of free monomers is depleted, so that $m(t_*) = 0$. At this time, the final cluster distribution is the one frozen at t_*, since no further attachments nor any detachments are possible. We shall call this the excess seed limit. Since the quantity $M - NN_s$ will play an important role in our analysis, we introduce the monomer excess parameter $\sigma = M/NN_s$, so that values of $\sigma \geqslant 1$ correspond to the excess monomer case, while $\sigma < 1$ describes the case of excess seeds.

To determine the final cluster-size distributions in both cases, first note that Eqs. (1) [or Eqs. (4)] are nonlinear due to the constraint on $m(t)$ involving $c_k(t)$ via Eq. (2). If $q_k = 0$, however, all terms on the right-hand side multiply $m(t)$. We can make analytic progress by dividing by $m(t)$ and defining a rescaled time τ according to

$$\frac{d\tau}{dt} = m(t) = M - \sum_{k=1}^{N} kc_k(t). \quad (5)$$

Equations (1) can now be written as

$$\begin{aligned} \frac{dc_0}{d\tau} &= -p_0 c_0, \\ \frac{dc_k}{d\tau} &= p_{k-1}c_{k-1} - p_k c_k, \\ \frac{dc_N}{d\tau} &= p_{N-1}c_{N-1}. \end{aligned} \quad (6)$$

Our goal is to find the rescaled time τ_* corresponding to the rescaled time at which monomers are irreversibly depleted: $m(\tau_*) = M - \sum_{k=1}^{N} kc_k(\tau_*) = 0$. The quenched, steady-state cluster-size distribution is thus found by evaluating the cluster concentrations at τ_*: $c_k(\tau_*) \equiv c_k^*$. Equations (6) are linear and can be solved by using Laplace transforms. Upon defining $\tilde{c}_k(s) = \int_0^\infty e^{-s\tau} c_k(\tau) d\tau$, we find that $\tilde{c}_k(s)$ satisfy

$$\begin{aligned} s\tilde{c}_0 - N_s &= -p_0 \tilde{c}_0, \\ s\tilde{c}_k &= -p_k \tilde{c}_k + p_{k-1}\tilde{c}_{k-1}, \\ s\tilde{c}_N &= p_{N-1}\tilde{c}_{N-1}, \end{aligned} \quad (7)$$

which yield the solutions

$$\frac{\tilde{c}_k(s)}{N_s} = \frac{\prod_{j=0}^{k-1} p_j}{\prod_{j=0}^{k}(s+p_j)}, \quad \frac{\tilde{c}_N(s)}{N_s} = \frac{\prod_{j=0}^{N-1} p_j}{s\prod_{j=0}^{N-1}(s+p_j)}. \quad (8)$$

To simplify our analysis, we restrict ourselves to uniform intrinsic attachment rates $p_k = p$ and use units of time such that $p = 1$. The dynamics are now described by Eq. (4) with $\varepsilon = 0$. The solutions represented by Eqs. (8) thus simplify to

$$\frac{\tilde{c}_k(s)}{N_s} = \frac{1}{(s+1)^{k+1}}, \quad \frac{\tilde{c}_N(s)}{N_s} = \frac{1}{s(s+1)^N}, \quad (9)$$

which can be inverse Laplace transformed to yield

$$\frac{c_{k<N}(\tau)}{N_s} = \frac{\tau^k e^{-\tau}}{k!}, \quad \frac{c_N(\tau)}{N_s} = 1 - \sum_{j=0}^{N-1} \frac{\tau^j e^{-\tau}}{j!}. \quad (10)$$

These results obey the constraint in Eq. (3). The value of τ_* can now be found by using Eqs. (10) in the mass constraint Eq. (2)

and imposing the condition $m(\tau_*) = 0$. After some algebra, this condition yields

$$\frac{\tau_*^N e^{-\tau_*}}{N\Gamma(N)} + (N - \tau_*)\frac{\Gamma(N, \tau_*)}{N\Gamma(N)} = 1 - \sigma. \quad (11)$$

As mentioned above, we expect a finite solution τ_* only in the excess seed ($\sigma < 1$) case. For excess monomers ($\sigma \geqslant 1$), we do not expect a finite time at which monomers are depleted. Indeed, the left-hand side of the above expression is positive and monotonically decreasing, implying that Eq. (11) will have a finite, real solution only in the excess seed case, for $\sigma < 1$. When the initial monomer number M is increased, and σ decreases past unity, the root τ_* diverges since all binding sites on the seeds are eventually occupied and further depletion of monomers can never occur. The quenched concentrations in this case are described by $m(\tau_* \to \infty) = M - NN_s$ and $c_k(\tau_* \to \infty) = N_s \delta_{k,N}$, indicating that all seeds are filled to capacity for $\sigma \geqslant 1$, as expected.

As a nontrivial example of the excess seed case, $\sigma < 1$, we can numerically solve Eq. (11) for $N = 10$, $M = 30$, $N_s = 8$, and $\sigma = 3/8$ to obtain $\tau_* = 3.75248$ and

$$\begin{aligned} \frac{c_0}{N_s} &= e^{-\tau_*} = 0.02346, \quad \frac{c_1}{N_s} = \tau_* e^{-\tau_*} = 0.088031, \\ \frac{c_2}{N_s} &= \frac{\tau_*^2}{2!}e^{-\tau_*} = 0.165168, \quad \frac{c_3}{N_s} = \frac{\tau_*^3}{3!}e^{-\tau_*} = 0.206596, \\ \frac{c_4}{N_s} &= \frac{\tau_*^4}{4!}e^{-\tau_*} = 0.193812, \quad \frac{c_5}{N_s} = \frac{\tau_*^5}{5!}e^{-\tau_*} = 0.145455, \\ \frac{c_6}{N_s} &= \frac{\tau_*^6}{6!}e^{-\tau_*} = 0.0909699, \quad \frac{c_7}{N_s} = \frac{\tau_*^7}{7!}e^{-\tau_*} = 0.0487661, \\ \frac{c_8}{N_s} &= \frac{\tau_*^8}{8!}e^{-\tau_*} = 0.0228743, \quad \frac{c_9}{N_s} = \frac{\tau_*^9}{9!}e^{-\tau_*} = 0.0095373, \\ \frac{c_{10}}{N_s} &= \frac{\tau_*^{10}}{10!}e^{-\tau_*} = 0.0035788. \end{aligned} \quad (12)$$

It can be explicitly verified that these solutions obey $\sum_{k=0}^{10} c_k^* = N_s$. Finally, for large N (but $N_s N < M$), the root of Eq. (11) is approximately

$$\tau_* \simeq \frac{M}{N_s} + \frac{e^{-\frac{M}{N_s}} N_s}{M\sqrt{2\pi N}}\left(\frac{eM}{NN_s}\right)^N, \quad (13)$$

which allows us to find analytic approximations to the final quenched values $c_k^* = c_k(\tau_*)$ in this limit. The full irreversible dynamics are illustrated in Fig. 2. In order to find approximations for the maximal concentrations of clusters $c_k(t)$ of size $k < N$, we note that from Eq. (10) they occur at the rescaled time $\tau_{\max} = k$. To find the corresponding real time $t_{\max}$ we insert Eqs. (10) into the scaling relationship Eq. (5) so that

$$\frac{d\tau}{dt} = M - N_s \sum_{k=1}^{N-1} k\frac{\tau^k e^{-\tau}}{k!} - N\left(1 - \sum_{k=0}^{N-1} \frac{\tau^k e^{-\tau}}{k!}\right). \quad (14)$$

Equation (14) can be numerically integrated to find $t(\tau)$. An approximation can be easily derived for large N (while
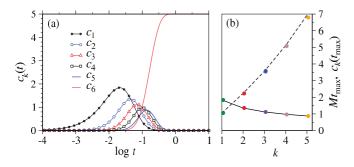
FIG. 2. (Color online) (a) Numerical solution to Eqs. (4) with $M = 50$, $N = 6$, $N_s = 5$, and $\varepsilon = 0$. Since monomers are in excess ($\sigma = 5/3 > 1$), all clusters except c_N vanish at long times. This plot is indistinguishable from the one plotted using $\varepsilon = 0.0001$, and is qualitatively similar to what would be found for a constant free monomer concentration $m(t) = M$. (b) The numerically computed (colored dots) maximal cluster concentrations $c_k(t_{\max}) = k^k e^{-k}/k!$ and corresponding times $t_{\max}$. The approximation $t_{\max} \approx N_s^{-1} \ln[M/(M - N_s k)]$ and the corresponding $c_k(t_{\max})$ are also shown by the dashed and solid curves, respectively.

remaining in the $N_s N < M$ excess monomer limit). In this case, the right-hand side of Eq. (14) is approximately

$$\sum_{k=1}^{N-1} k \frac{\tau^k e^{-\tau}}{k!} \approx \tau, \tag{15}$$

with corrections of $O(1/N)$. Equation (14) can therefore be accurately approximated by

$$\frac{d\tau}{dt} \approx M - N_s \tau, \tag{16}$$

which can be explicitly integrated to give

$$t(\tau) \approx N_s^{-1} \ln[M/(M - N_s \tau)]. \tag{17}$$

We plot $t_{\max} \equiv t(\tau_{\max}) = t(k) \approx N_s^{-1} \ln[M/(M - N_s k)]$ and the associated $c_k(t_{\max}) = k^k e^{-k}/k!$ in Fig. 2(b) as a function of k. The approximation for $t_{\max}$ is shown by the dashed curve in Fig. 2(b) and is extremely accurate, especially for small k where maxima are reached before appreciable accumulation of larger clusters invalidate the approximation $\dot{\tau} \approx M - N_s \tau$.

In the next section we will analyze the nucleation process when successive monomer detachment is allowed. The question will arise as to how closely the irreversible nucleation results found here are followed in the case of a vanishingly small, but nonzero, detachment rate ε. As we shall see, our reversible results will closely mirror the irreversible ones in the limit $\varepsilon \to 0^+$, *only* in the excess monomer case, when seeds are saturated with ligands. In the excess seed case on the other hand, dramatic differences between reversible and irreversible binding arise, even as $\varepsilon \to 0^+$. Only very special parameter choices will lead to the rare matching of reversible and irreversible dynamics for specific clusters.

IV. REVERSIBLE BINDING

In this section we find the equilibrium cluster-size distributions allowing for positive detachment rates $q_k > 0$. We start by finding the equilibrium cluster concentrations $c_k^{\text{eq}} \equiv c_k(t \to \infty)$ by setting $dc_k/dt = 0$ in Eqs. (1). Due to

reversibility, initial conditions are irrelevant. After defining $m^{\text{eq}} \equiv M - \sum_{k=1}^{N} k c_k^{\text{eq}}$, we find that c_k^{eq} can be written as a function of c_0^{eq} and m^{eq} as follows:

$$c_k^{\text{eq}} = c_0^{\text{eq}} \frac{\prod_{j=0}^{k-1} p_j}{\prod_{j=1}^{k} q_j} [m^{\text{eq}}]^k. \tag{18}$$

This expression can be used in the mass constraint of Eq. (2) and the total cluster number constraint in Eq. (3) to find two equations for the two unknowns c_0^{eq} and m^{eq}:

$$m^{\text{eq}} = M - c_0^{\text{eq}} \sum_{k=1}^{N} k \frac{\prod_{j=0}^{k-1} p_j}{\prod_{j=1}^{k} q_j} [m^{\text{eq}}]^k, \tag{19}$$

$$N_s = c_0^{\text{eq}} \sum_{k=1}^{N} \frac{\prod_{j=0}^{k-1} p_j}{\prod_{j=1}^{k} q_j} [m^{\text{eq}}]^k. \tag{20}$$

These equations can be solved by substituting the expression for c_0^{eq} in Eq. (20) into Eq. (19) and determining m^{eq} numerically. Again, computations are greatly simplified by restricting our analysis to uniform attachment and detachment rates $p_k = p$ and $q_k = q$, respectively. Further nondimensionalizing time in units of p^{-1} and introducing $\varepsilon \equiv q/p$, Eqs. (18) become

$$c_k^{\text{eq}} = c_0^{\text{eq}} \left[\frac{m^{\text{eq}}}{\varepsilon} \right]^k \equiv c_0^{\text{eq}} z^k, \tag{21}$$

where $z \equiv m^{\text{eq}}/\varepsilon$. The fixed seed number constraint in Eq. (3) yields $c_0^{\text{eq}} = N_s(z - 1)/(z^{N+1} - 1)$ so that by substituting $c_0^{\text{eq}} z^k$ into Eq. (2) we find an equation for z:

$$\left(\frac{\varepsilon z}{N_s N} - \sigma \right)(z - 1)(z^{N+1} - 1) + z^{N+2}$$
$$- (1 + 1/N)z^{N+1} + \frac{z}{N} = 0. \tag{22}$$

Equation (22) determines the numerical value for the normalized cluster fugacity z. In the small detachment limit $\varepsilon \to 0^+$, once more, the two limits of excess monomers and excess seeds naturally arise. In the excess monomer case, $\sigma \geqslant 1$, the real root of Eq. (22) can be found as the inner solution of a singular perturbation [27], where the largest power of z multiplies ε so that $z = \varepsilon^{-1}(M - N_s N) + N_s(M - N_s N)^{-1} + O(\varepsilon)$. Inserting this approximation for z into the seed constraint Eq. (3), we find $c_0^{\text{eq}} \approx N_s[\varepsilon/(M - N_s N)]^N + O(\varepsilon)$, which yields

$$c_k^{\text{eq}} \approx \frac{N_s}{(N_s N)^{N-k}} \frac{\varepsilon^{N-k}}{(\sigma - 1)^{N-k}} + O(\varepsilon^{N-k+1}). \tag{23}$$

Thus, equilibrium concentrations all vanish as $O(\varepsilon^{N-k})$ except that of the maximum cluster $k = N$, which asymptotes to $c_N^{\text{eq}} \approx N_s - O(\varepsilon)$. This qualitative behavior is expected in the excess monomer case when nearly all available binding sites are occupied and only nearly fully occupied seeds survive. In particular, when $\varepsilon \to 0^+$, $c_{k \neq N}^{\text{eq}} \to 0$ and $c_N^{\text{eq}} \to N_s$. This result is identical to what was found for the strictly irreversible case of $\varepsilon = 0$ in the preceding section. Thus, in the excess monomer case ($\sigma \geqslant 1$), all clusters will be filled to capacity in the case of vanishingly small detachment rates, regardless of when the limit $\varepsilon \to 0^+$ is taken.
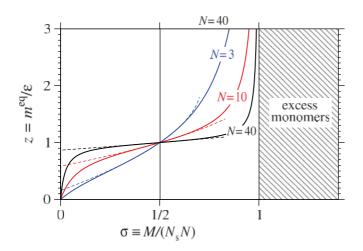
FIG. 3. (Color online) Values of the normalized cluster fugacity z determined from the real root of Eq. (22). Fugacities for $N = 3, 10, 40$ are plotted in the limit $\varepsilon/(N_s N) = 10^{-6}$. A good approximation to z is given by Eq. (24) and is shown by the dashed curves. The region $\sigma \equiv M/(N_s N) \geqslant 1$ corresponds to the case of excess monomers where $c_k^{\mathrm{eq}} \sim \varepsilon^{N-k}$, as shown in Eq. (23).

In the opposite case of excess seeds, $\sigma < 1$, monomers are depleted before all binding sites on all N_s seeds can be filled, leading to finite concentrations c_k^{eq}. Interestingly, the excess seed limit *further separates into two subcases*. From our numerical analysis of Eq. (22) we find that $z > 1$ for $1/2 < \sigma < 1$, implying that $c_{k+1}^{\mathrm{eq}} > c_k^{\mathrm{eq}}$ and larger cluster sizes tend to be favored. On the contrary, for $\sigma < 1/2$ we find $z < 1$ so that $c_{k+1}^{\mathrm{eq}} < c_k^{\mathrm{eq}}$. In this case, there are too few monomers M for larger clusters to persist and smaller cluster sizes are more populated. For a range of values of σ near $1/2$ we find that the approximation

$$z \approx 2 - \left[1 - \frac{24}{N+2} \left(\sigma - \frac{1}{2} \right) \right]^{1/2}, \qquad (24)$$

and the associated $c_k^{\mathrm{eq}} = c_0^{\mathrm{eq}}(z) z^k$, are highly accurate. Note that at the special point $\sigma = 1/2$ the monomer fugacity $z = 1$ and all equilibrium concentrations $c_k^{\mathrm{eq}} = N_s/(N+1)$ are equal. The behavior of the root z of Eq. (22) as a function of the monomer excess is plotted for $\sigma < 1$ in Fig. 3. The analytic approximation Eq. (24) is also indicated by the dashed curves.

Our analysis thus far does not provide insight into *how* the equilibrium state is reached. As discussed earlier, when $\varepsilon \to 0^+$, we expect binding to occur in a nearly irreversible manner over intermediate times, yielding metastable cluster-size distributions. Repeated monomer detachment and reattachment become significant only after much longer times, of the order $t_c \sim \varepsilon^{-1}$, allowing redistribution of mass into equilibrium clusters.

To find the metastable cluster-size distribution, we make the *ansatz* that $c_k(t)$ can be approximated by setting the detachment rate $\varepsilon = 0$ at intermediate times. We may thus neglect detachment and use the results obtained for irreversible binding up to $t_c \sim \varepsilon^{-1}$, beyond which detachment effects may become appreciable, both in the excess monomer and excess seed cases.

Figure 2(a) shows the full time dependence of $c_k(t)$ in the reversible, excess monomer case where $\sigma = 5/3 \geqslant 1$. Here, as expected, both $c_{k<N}^{\mathrm{eq}}$ and $c_{k<N}(\tau \to \infty) \equiv c_{k<N}^*$ vanish as $\varepsilon \to 0^+$. In this case, the dynamics is not appreciably affected by the onset of detachment and there are no dramatic behavioral crossovers originating across the ε^{-1} time scale. Reversible and irreversible dynamics thus coincide at all time scales in the $\varepsilon \to 0^+$ limit if $\sigma \geqslant 1$. In particular, the initial rise in $c_{0<k\leqslant N}(t)$ is determined by the monomer loading process and is independent of the detachment rate ε. Setting $\varepsilon = 0$ and using our results from the preceding section we can numerically compute the time scale $t_{\max}$ over which the cluster-size distributions peak. We have verified that as $\varepsilon \to 0^+$, the full dynamics arising from the reversible binding process is not appreciably different from that obtained in the irreversible binding limit. In summary, when monomers are in excess, $\sigma \geqslant 1$, the differences between c_k^{eq} and c_k^* vanish in the $\varepsilon \to 0^+$ limit, ergodicity-breaking is not apparent, and seeds are always filled to capacity.

We now consider reversible binding in the $\sigma < 1$ case, where there are more receptor seeds than initial free monomers. As in the *ansatz* made in the excess monomer case, we assume that at least up to time scales of order ε^{-1}, the dynamics can be approximated as an irreversible binding process, where $\varepsilon = 0$. By following the full dynamics in Eqs. (4) we verify that at intermediate times, the metastable concentrations $c_k(t)$ approach levels approximated by the final ones $c_k(\tau_*) \equiv c_k^* \equiv N_s \tau_*^k e^{-\tau_*}/k!$ reached in the irreversible case when $\varepsilon = 0$. Following the evolution of Eqs. (4) beyond time scales ε^{-1}, we find that these metastable concentrations eventually coarsen toward a qualitatively different equilibrium distribution defined by $c_k^{\mathrm{eq}}(\varepsilon \to 0^+)$.

This qualitative difference in cluster-size distributions is noticeable *only* in the excess seed limit when $\sigma < 1$ and illustrates ergodicity-breaking at $\varepsilon = 0$, as clearly shown in Fig. 4. In Fig. 4(a), where $\sigma = 3/8 < 1/2$, seeds are in such strong excess that monomers are quickly depleted and $c_{k+1}^* < c_k^*$. Figure 4(b) plots c_k^{eq} as a function of ε, found from numerically solving Eq. (22). Note that the values of $c_k^{\mathrm{eq}}(\varepsilon \to 0^+)$ differ from the intermediate ones approximated by the frozen distribution c_k^*. The latter are indicated by the colored dots. Figures 4(c) and 4(d) are the analogous plots but for $1/2 < \sigma < 1$, where $c_{k+1}^* > c_k^*$. When seeds are in excess, the crossover to equilibrium is clearly observable over the coarsening time scale $t_c \sim \varepsilon^{-1}$.

V. APPARENT ACCELERATED EQUILIBRATION OF SPECIFIC CLUSTERS

The general qualitative behavior described in the preceding section is that when seeds are in excess ($\sigma < 1$), the full heterogeneous nucleation problem exhibits dynamics occurring over two time scales. The first is of $t \sim O(1)$ and corresponds to monomer attachment rates, while the second coarsening time scale, $t_c \sim \varepsilon^{-1}$, is associated with the monomer detachment rate. In general, $c_k^{\mathrm{eq}} \neq c_k^*$.

However, upon fine tuning relevant parameters, we find special values of $\sigma < 1$ and N where up to two specific cluster sizes k can have nearly equal values of quenched and equilibrium concentrations ($c_k^{\mathrm{eq}} \approx c_k^*$) in the $\varepsilon \to 0^+$ limit.
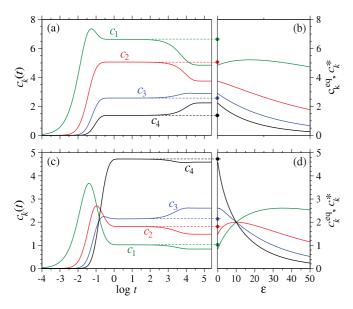
FIG. 4. (Color online) Ergodicity-breaking occurs only when seeds are in excess. (a) Numerical solution to Eqs. (4) with $\varepsilon = 0.0001$, $M = 30$, $N = 4$, and $N_s = 20$ ($\sigma = 3/8$). In this strong excess seed case, $\sigma < 1/2$ and both $c_k^* > c_{k+1}^*$ and $c_k^{eq} > c_{k+1}^{eq}$. (b) c_k^{eq} as a function of ε. Note that even as $\varepsilon \to 0^+$, c_k^{eq} are different from the metastable values c_k^* (colored dots) found from setting $\varepsilon = 0$ in Eqs. (4). (c) Cluster concentrations $c_k(t)$ for $\varepsilon = 0.0001$, $M = 30$, $N = 4$, and $N_s = 10$ ($\sigma = 3/4$). In this weak excess seed case, $\sigma > 1/2$, both $c_k^* < c_{k+1}^*$ and $c_k^{eq} < c_{k+1}^{eq}$. (d) Again, ergodicity-breaking arises since $c_k^{eq}(\varepsilon \to 0) \not\to c_k^*(\varepsilon \to 0)$. In all plots, the free monomer concentration $m(t)$ and the number of naked seeds $c_0(t)$ can be reconstructed from the constraint conditions and are not explicitly shown. Labeling for panels (b) and (d) is such that the c_k^{eq} values at $\varepsilon = 0$ correspond to the closest c_k values in panels (a) and (c), respectively.

These clusters quickly reach their equilibrium concentrations on a short time scale independent of ε. Mathematically, the sizes k that are subjected to this rapid, apparent equilibration can be found by setting $c_k^* = c_k^{eq}$:

$$N_s \frac{\tau_*^k e^{-\tau_*}}{k!} = N_s \frac{(z-1)z^k}{(z^{N+1}-1)}, \qquad (25)$$

where τ_* and z are determined by Eqs. (11) and (22), respectively.

Figure 5(a) shows the relative difference $(c_k^* - c_k^{eq})/c_k^{eq}$ for fixed $N = 6$ and σ as a function of the discrete cluster size k. Generally, we find that many values of $0 < \sigma < 1$ give rise to at least one value of k at which quenched cluster concentrations equal equilibrium concentrations. In the above example, $N = 6$ and $\sigma = 0.35633$, and clusters of size $k = 4$ (red arrow) quickly quench to their equilibrium values. Figure 5(b) plots the numerical solution to Eq. (4) for $\varepsilon = 10^{-10}$, $N = 6$ and $\sigma = 0.35633$. For simplicity, we have plotted only $c_3(t), c_4(t)$, and $c_5(t)$. Note that even though $c_4^* = c_4^{eq}$ (dashed line), $c_4(t)$ does suffer a small transient perturbation due to the rearrangement of all other clusters $c_{k\neq4}$ at time $t \sim \varepsilon^{-1}$, temporarily disturbing the balance of $c_4(t)$. Figures 5(c) and 5(d) illustrate the behavior for $\sigma = 0.86293$. Here, Fig. 5(c) predicts that c_1 quickly reaches its equilibrium value. Figure 5(d) explicitly plots $c_0(t), c_1(t)$, and $c_2(t)$ for $\sigma = 0.86293$. Figures 5(a)
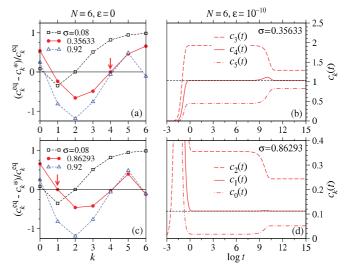

FIG. 5. (Color online) (a) The relative difference $(c_k^* - c_k^{eq})/c_k^{eq}$ as a function of discrete values of k for $\sigma = 0.08, 0.35633, 0.92$. (b) Selected cluster concentrations for $\sigma \equiv M/(N_s N) = 0.35633$, where $c_{k=4}^* \approx c_{k=4}^{eq}$. Note the small transient in $c_4(t)$ near $t \sim \varepsilon^{-1}$. (c) $(c_k^* - c_k^{eq})/c_k^{eq}$ plotted as a function of k for $\sigma = 0.08, 0.86293, 0.92$ These values indicate that for $\sigma = 0.86293$, the concentration $c_1(t)$ quickly reaches its equilibrium value. (d) The corresponding concentration plot showing just $c_0(t), c_1(t)$, and $c_2(t)$. These plots also indicate that for $\sigma = 0.08$, the concentration $c_2(t)$ experiences accelerated equilibration.

and 5(c) also suggest that $c_4^* \approx c_4^{eq}$ over a wide range of values of σ. For the finite processes we have considered, we find that at most two sizes of k, out of N, can exhibit accelerated equilibration, provided σ and N are precisely tuned. We expect the qualitative aspects of these results to hold when binding and/or unbinding rates are weakly cluster-size dependent, allowing our analysis to apply in scenarios of weakly cooperative ligand-receptor binding [24].

VI. CONCLUSIONS

In this work we have analyzed a simple and mathematically tractable model of heterogeneous nucleation to describe ligand-receptor binding in closed systems, such as within cells or organelles. A complete analysis in terms of the parameters (M, N, N_s) in the $\varepsilon \to 0^+$ limit shows how dramatically differently the system behaves in a monomer-rich environment compared to a seed-rich one. In the latter case, when binding sites outnumber initial monomers ($\sigma < 1$), we find that after an initial transient $\sim t_{max}$, cluster densities first approach c_k^*, approximating the quenched concentrations when $\varepsilon = 0$ and all free monomers have been depleted. This long-lived metastable distribution eventually coarsens to a very different equilibrium distribution c_k^{eq} at much later times $t_c \sim 1/\varepsilon$. Surprisingly, when parameters (σ and N) are finely tuned, it is also possible that $c_k^* \approx c_k^{eq}$, for particular k clusters, resulting in much shorter coarsening times. We find that clusters of up to two specific sizes may appear to reach their equilibrium concentrations by $t \sim (1)$. Our results have general implications for ligand-receptor kinetics and suggest practical ways of tuning (M, N, N_s) in experiments to

accelerate the equilibration of specific clusters by stabilizing their metastable sizes.

There are potentially many physical realizations of our analysis. In the hemoglobin example mentioned in the Introduction, N_s would correspond to the concentration of oxygen-binding hemoglobin metalloproteins, while M would represent the oxygen molecule concentration. Here, each hemoglobin binds at most $N = 4$ oxygen molecules, and typically there is an excess of oxygen ligands ($M \gg N_s N$), except perhaps under the most extremely hypoxic conditions. However, there are many other scenarios in which ligand concentrations can be comparable or lower than the total number of binding sites ($M \sim N_s N$). Examples where ligand depletion often occurs include transcription factor binding, radioligand analysis [28,29], and signal transduction [30]. In this last example, the dynamic range of receptor concentrations predicted by our analysis puts bounds on the chemical signaling that can arise from up-regulation of receptor expression.

A number of extensions of our analysis can be further investigated. Certain forms for cluster-size-dependent attachment and detachment rates, p_k and q_k, can be incorporated into the analysis. For example, if $p_k \sim k$, certain products and sums in Eqs. (18), (19), and (20) can be analytically expressed or approximated to derive variations to Eq. (22) and the associated concentrations c_k^{eq}. Furthermore, for small numbers of clusters, the mean-field results derived from the Becker-Döring equations may deviate from the expected cluster-size distributions arising from fully stochastic simulations [22]. We expect our mean-field results to be qualitatively valid when cluster correlations are included in the dynamics. A careful quantitative investigation of stochastic effects will be included in future work.

[1] C. M. Losert-Valiente Kroon and I. J. Ford, Atmos. Res. doi:10.1016/j.atmosres.2010.12.019 (2011).

[2] M. Lazaridis, O. Hov, and K. Eleftheriadis, Atmos. Res. **55**, 103 (2000).

[3] P. M. Winkler *et al.*, Science **319**, 1374 (2008).

[4] J. Schmelzer, *Nucleation Theory and Applications* (Wiley-VCH Verlag, Weinheim, Germany, 2005).

[5] E. Ruckenstein and Y. S. Djikaev, Adv. Colloid Interface Sci. **118**, 561 (2005).

[6] F. A. Ferrone, M. Ivanova, and R. Jasuja, Biophys. J. **82**, 399 (2002).

[7] A. Lomakin, D. S. Chung, G. B. Benedek, D. A. Kirschner, and D. B. Teplow, Proc. Natl. Acad. Sci. USA **93**, 1125 (1996).

[8] M. J. Dayel and R. D. Mullins, PLoS Biol. **2**(4), e91 (2004).

[9] M. G. J. Ford *et al.*, Science **291**, 1051 (2001).

[10] C. Walsh, *Enzymatic Reaction Mechanisms* (W. H. Freeman, New York, 1979).

[11] M. Gibbons, T. Chou, and M. R. D'Orsogna, J. Phys. Chem. B **114**, 15403 (2010).

[12] T. Yoneyama and K. Hatakeyama, Protein Sci. **10**, 871 (2001).

[13] L. J. Cook, R. K. P. Zia, and B. Schmittmann, Phys. Rev. E **80**, 031142 (2009).

[14] J. A. D. Wattis and J. R. King, J. Phys. A **31**, 7169 (1998).

[15] O. Penrose, J. Stat. Phys. **89**, 305 (1997).

[16] P. Krapivsky, E. Ben-Naim, and S. Redner, *Statistical Physics of Irreversible Processes* (Cambridge University Press, Cambridge, United Kingdom, 2008).

[17] M. Lazaridis and I. J. Ford, J. Chem. Phys. **99**, 5426 (1993).

[18] N. H. Fletcher, J. Chem. Phys. **29**, 572 (1958).

[19] B. N. Hale and J. Kiefer, J. Stat. Phys. **12**, 437 (1975).

[20] B. Nowakowski and E. Ruckenstein, J. Phys. Chem. **96**, 2313 (1992).

[21] Y. Farjoun and J. C. Neu, Phys. Rev. E **78**, 051402 (2008).

[22] J. S. Bhatt and I. J. Ford, J. Chem. Phys. **118**, 3166 (2003).

[23] P. Smereka, J. Stat. Phys. **132**, 519 (2008).

[24] M. R. D'Orsogna and T. Chou, Phys. Rev. Lett. **95**, 170603 (2005).

[25] S. N. Majumdar, S. Krishnamurthy, and M. Barma, Phys. Rev. Lett. **81**, 3691 (1998).

[26] B. Niethammer, J. Nonlinear Sci. **13**, 115 (2008).

[27] C. M. Bender and S. A. Orzag, *Advanced Mathematical Methods for Scientists and Engineers: Asymptotic Methods and Perturbation Theory* (Springer, New York, 1999).

[28] S. Swillens, Mol. Pharmacol. **47**, 1197 (1995).

[29] A. Goldstein and R. W. Barrett, Mol. Pharmacol. **31**, 603 (1987).

[30] S. J. Edelstein, M. I. Stefan, and N. Le Novère, PLoS ONE **5**, e8449 (2010).